FRAGMENT OF A BED STRUCTURE 03 12751-20.2.5 - TIN BRONZE - ROMAN TIMES - SWITZERLAND

Artefact name	Fragment of a bed structure 03 12751-20.2.5
Authors	Marianne. Senn (Empa, Dübendorf, Zurich, Switzerland) & Christian. Degrigny (HE-Arc CR, Neuchâtel, Neuchâtel, Switzerland)
Url	/artefacts/922/

The object

Credit HE-Arc CR.

Fig. 1: Fragment from a bed structure (after Krieg, conservation project report, 2009, 25),

Description and visual observation

Description of the artefact	Fragment from a series of 9 elements of a Roman bed structure, covered with green-black corrosion products (Fig. 1).
Type of artefact	Furniture element
Origin	"Palais de Derrière la Tour", Avenches, Vaud, Switzerland
Recovering date	Excavation 2003
Chronology category	Roman Times
chronology tpq	150 A.D.
chronology taq	200 A.D.
Chronology comment	Second half of the 2nd Century AD

This work is licensed under CC BY-NC-ND 4.0

Burial conditions / environment	Soil
Artefact location	Roman museum, Avenches, Vaud
Owner	Roman museum, Avenches, Vaud
Inv. number	03/12751-20.2.5
Recorded conservation data	N/A

Complementary information

The metal underneath the green-black corrosion layers is decorated with incrustations (Ag and Cu) representing meanders and olive branches. An intentional black patina might have been applied on the ancient surface to contrast it with the silver and pink coloured inlays.

Study area(s)

Credit HE-Arc CR.

Fig. 2: Location of sampling area,

Binocular observation and representation of the corrosion structure

None.

MiCorr stratigraphy(ies) – Bi

Sample(s)

This work is licensed under CC BY-NC-ND 4.0

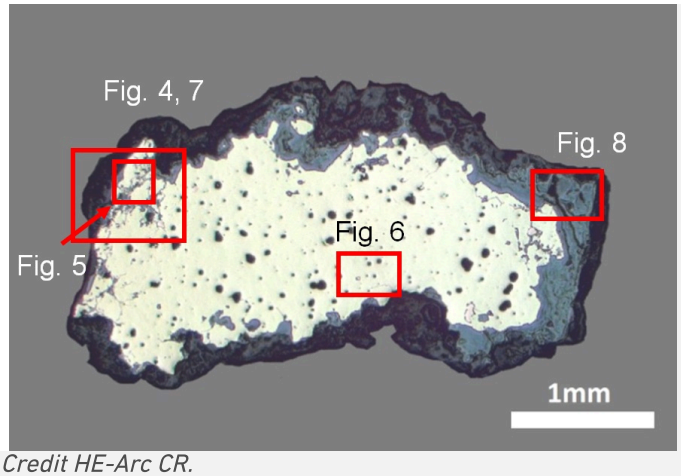

Credit HE-Arc CR.

Fig. 3: Micrograph, in bright field, of the cross-section of the sample taken from the bed structure showing the location of Figs. 4 to 8,

Description of sample	The sample is a section from the fragment represented on Fig. 2. The remaining metal is surrounded by a thick corrosion crust (Fig. 3). Its dimensions are: L = 3.5mm and W = 1.5mm.
Alloy	Tin Bronze
Technology	Partly annealed after cold working
Lab number of sample	HECR-MK5
Sample location	HE-Arc CR, La Chaux-de-Fonds, Neuchâtel
Responsible institution	HE-Arc CR, La Chaux-de-Fonds, Neuchâtel
Date and aim of sampling	2008-2009, analyses of the corrosion products

Complementary information

None.

Analyses and results

Analyses performed:
Metallography (etched with ferric chloride reagent), Vickers hardness testing, SEM/EDS, XRD, Raman spectroscopy.

Non invasive analysis

None.

Metal

This work is licensed under CC BY-NC-ND 4.0

The remaining metal is a porous tin bronze (Table 1) with tiny iron oxides inclusions (Table 2) and secondary re-deposited copper. Intergranular corrosion has developed locally inside the metal (Figs. 4 and 5). The etched alloy shows a structure principally consisting of large polygonal grains, some of which include strain lines (Fig. 6). Locally an isolated alpha + delta eutectoid can be seen. Much smaller twinned grains can be found on the left side of the sample (Fig. 5). The average hardness of the metal is HV1 100. However on the left side of the sample, where the grains are smaller and twinned, the hardness is much higher (more cold work followed by annealing).

Elements	Cu	Sn	Fe
mass%	82.0	13.0	?

Table 1: Chemical composition of the metal. Method of analysis: SEM/EDS, Lab of Electronic Microscopy and microanalysis, IMA (Néode), HEI Arc.

Elements	O	Mn	Fe	Cu	Sn	Total
Inclusions	23	0.7	64	8.7	1.8	99

Table 2: Chemical composition (mass %) of the tiny inclusions on Fig. 4. Method of analysis: SEM/EDS, Laboratory of Analytical Chemistry, Empa.

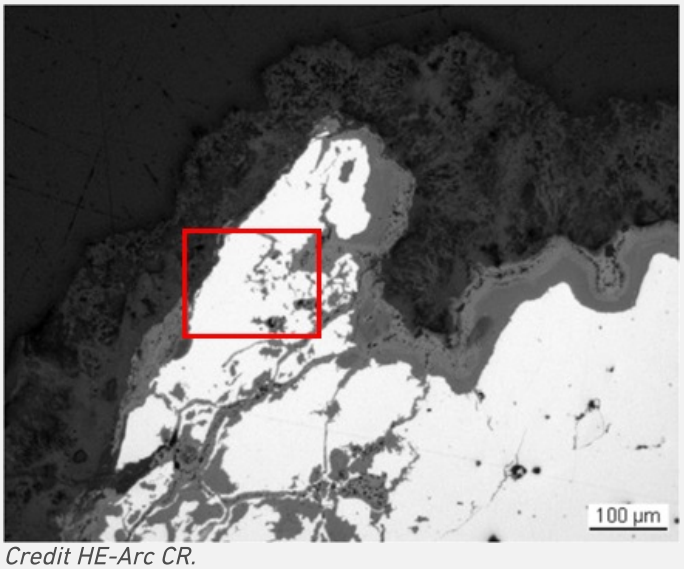

Credit HE-Arc CR.

Fig. 4: Micrograph of the metal sample from Fig. 3 (detail), unetched, bright field. From bottom right to top left we observe: the metal (in white) with porosity (in black) and the corrosion layer (in light and dark-grey). The micrograph of Fig. 5 is marked by a rectangle,

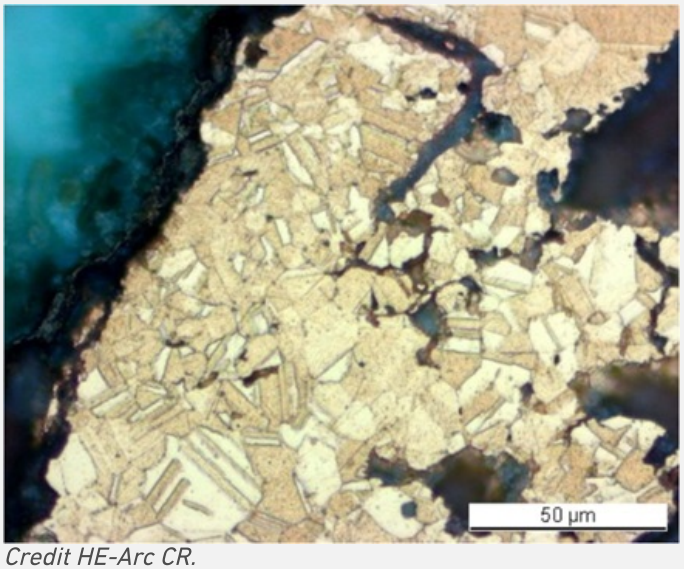

Credit HE-Arc CR.

Fig. 5: Micrograph of the metal sample from Fig. 3 (detail of Fig. 4), etched, bright field. The metal shows a structure of mostly small polygonal grains with twins,

This work is licensed under CC BY-NC-ND 4.0

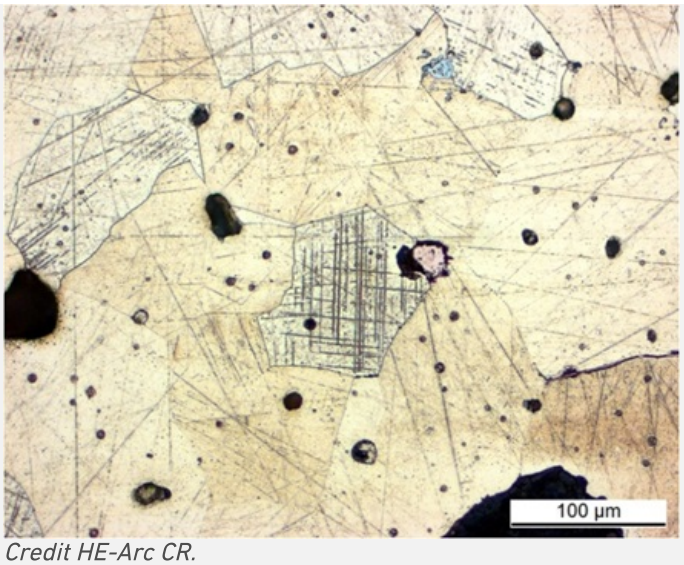

Credit HE-Arc CR.

Fig. 6: Micrograph of the metal sample from Fig. 3, etched, bright field. The metal shows a structure consisting of large polygonal grains including strain lines. Pores are in black, remnants of the Sn-rich eutectoid phase in grey and secondary deposited copper in pink,

Microstructure	Large and small polygonal grains with few twins + strain lines
First metal element	Cu
Other metal elements	Sn

Complementary information

None.

Corrosion layers

The metal - corrosion products interface is irregular (Fig. 3) and the average thickness of the corrosion crust is 300µm. The latter can be divided into four layers (Fig. 4). In bright field, the inner layer (CP4) is medium grey and dense. In polarised light it is dark-red/orange (Fig. 7). It is Sn-rich, contains O and Cl but is Cu depleted (Table 3 and Fig. 8). The next layer (CP3) is as well medium grey in bright field and light-red in polarised light. It has a composition similar to cuprite/Cu2O (Table 3). This was confirmed by Raman spectroscopy (Fig. 9). The third layer (CP2) is thin, is light grey in bright field and contains black pores. Under polarised light it looks brilliant black (Fig. 7) and is rich in Cu with Sn and O (Fig. 8). Using XRD, it was identified as a mixture of tenorite/CuO, cuprite/Cu2O and cassiterite/SnO2 (Krieg 2009). Raman spectroscopy could only detect tenorite in this layer (Fig. 10). In bright field the thick outer layer (CP1) is marbled in dark-grey and black, in polarised light it appears blue-green (Fig. 7). XRD analysis gave a composition close to malachite/Cu2CO3(OH)2 (Krieg 2009). In the present study no C was detected (Fig. 8), but Raman spectroscopy confirmed its presence (Fig. 11). The spectrum obtained shows a good match with published spectra (Bouchard and Smith 2003). Peaks are similar to those expected for malachite but most of them have a Raman shift: 3322, 1503, 1108, 1073, 759, 731, 603, 540, 442, 357, 276, 225, 186, 163 cm^{-1}. The underlined Raman shifts correspond to the peaks of greatest intensity. Environmental elements such as Si are concentrated on the top surface (Fig. 8).

Elements	O	Cu	Sn	Si	Cl	Mn	Fe	Pb	Total
CP3, red outer edge of the inner corrosion layer (average of 2 similar analyses)	19	69	5.1	0.7	<	<	<	<	94
CP4, dark-orange inner corrosion layer (average of 3 similar analyses)	25	52	25	0.9	0.6	<	<	1.0	104

Table 3: Chemical composition (mass %) of the corrosion crust from Fig. 7. Method of analysis: SEM/EDS, Laboratory of Analytical Chemistry, Empa.

This work is licensed under CC BY-NC-ND 4.0

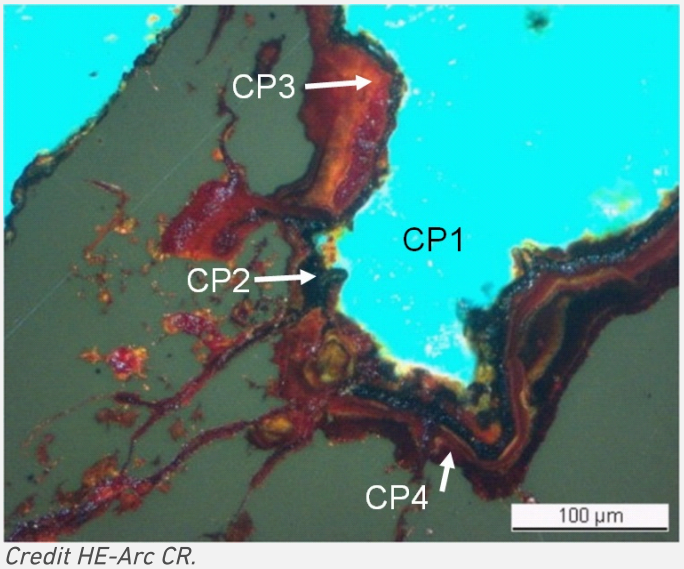

Credit HE-Arc CR.

Fig. 7: Micrograph showing the metal - corrosion crust interface from Fig. 3 (detail of Fig. 4) and corresponding to the stratigraphy of Fig. 12, polarised light. From bottom left to to right: In grey the metal, in dark-red/orange CP4, in light red CP3, in black (with pores) CP2 and in green-blue CP1,

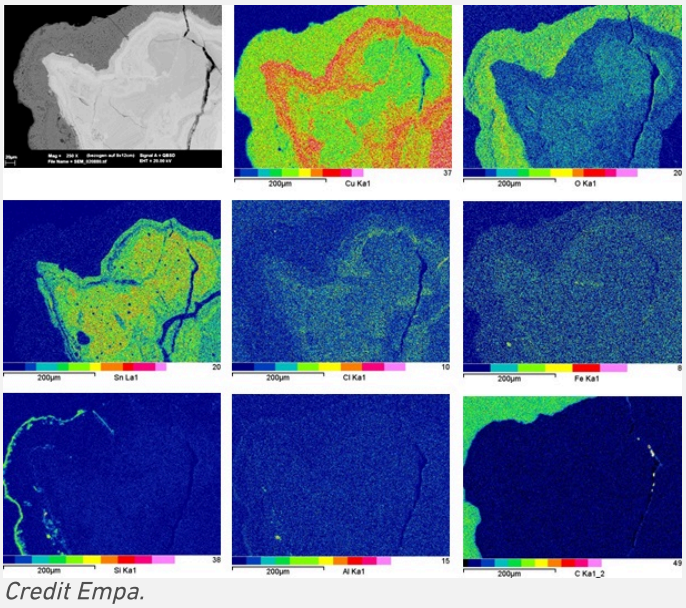

Credit Empa.

Fig. 8: SEM image, BSE-mode, and elemental chemical distribution of the selected area from Fig. 3 (reversed picture, detail). Method of examination: SEM/EDS, Laboratory of Analytical Chemistry, Empa,

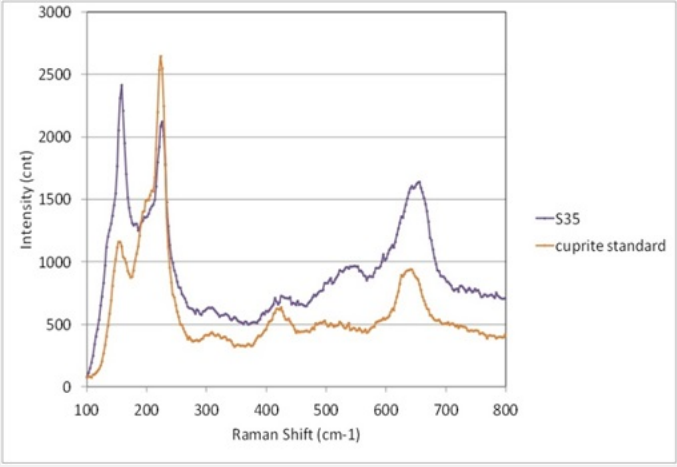

Credit SNM.

Fig. 9: Raman spectrum of CP3 (S35) from Fig. 7 compared to a cuprite standard spectrum. Settings: laser wavelength 532nm, acquisition time 20s, one accumulation, filter D2 (0.75-0.8mW), hole 1000, slit 100, grating 600. Method of analysis: Raman spectroscopy, Lab of Swiss National Museum, Affoltern a. Albis ZH,

This work is licensed under CC BY-NC-ND 4.0

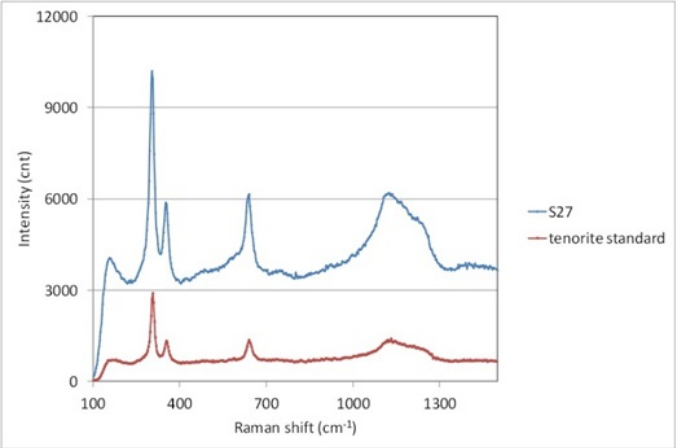

Credit SNM.

Fig. 10: Raman spectrum of the black layer (CP2) with pores (S27) from Fig. 7 compared to a tenorite standard spectrum. Settings: laser wavelength 532nm, acquisition time 100s, one accumulation, filter D1 (7.5-8mW), hole 500, slit 80, grating 600. Method of analysis: Raman spectroscopy, Lab of Swiss National Museum, Affoltern a. Albis ZH,

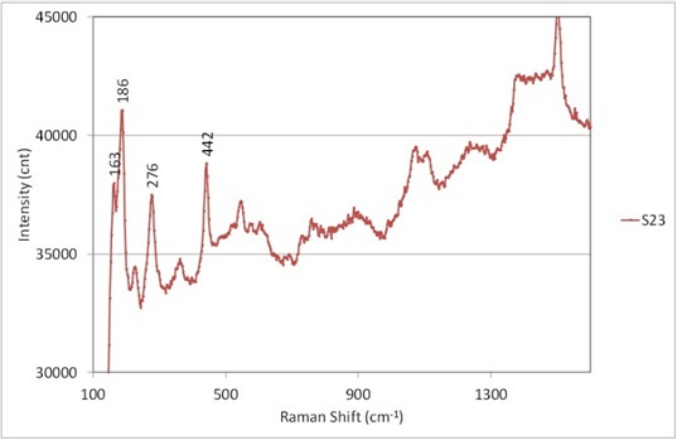

Credit SNM.

Fig. 11: Raman spectrum of the green outer corrosion layer (CP1) from Fig. 7. Settings: laser wavelength 532nm, acquisition time 80s, one accumulation, filter D2 (0.75-0.8mW), hole 500, slit 80, grating 600. Method of analysis: Raman spectroscopy, Lab of Swiss National Museum, Affoltern a. Albis ZH,

Corrosion form	Uniform - intergranular
Corrosion type	Type I or II ? (Robbiola)

Complementary information

None.

MiCorr stratigraphy(ies) – CS

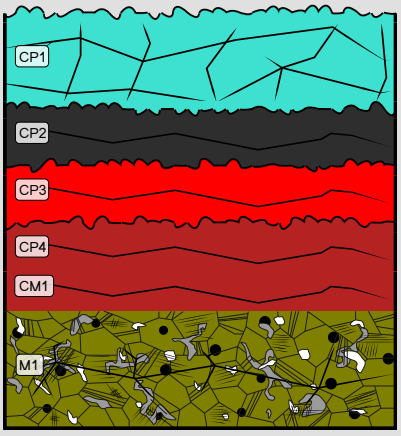

Fig. 12: Stratigraphic representation of the sample taken from the bed structure in cross-section (dark field) using the MiCorr application. The characteristics of the strata are only accessible by clicking on the drawing that redirects you to the search tool by stratigraphy representation. This representation can be compared to Fig. 7, Credit HE-Arc CR.

This work is licensed under CC BY-NC-ND 4.0

Synthesis of the binocular / cross-section examination of the corrosion structure

None.

Conclusion

One side of the tin bronze artefact has been repeatedly annealed after cold working whereas the rest of the metal was cold worked. The metal is covered with a terrestrial type corrosion layer. Cl is found in proximity to the metal in a Sn-rich but Cu-depleted inner area of the first cuprite layer. It is followed by an intermediate thin layer composed of a mixture of tenorite and tin oxides. The third voluminous layer is malachite. These results confirm Krieg's conclusions (Krieg 2009). Since the bed fragments have been excavated from a burnt down house, it is difficult to judge if the tenorite is an intentional black patina or if it is the result of heating during the fire. The limit of the original surface is outlined by the clear demarcation of Sn content (internal marker) in the first two corrosion layers and can be located between layers 2 & 3. Intentional or no, the black tenorite/cassiterite layer most likely represents the surface that will retain most surface details. In this case, the corrosion type is difficult to attribute after Robbiola et al. 1998.

References

References on object and sample

Reference object

1. Delbarre-Bärtschi, S., Fischbacher, V., Krieg, M. (2009) Lits en bronze à Avenches: état de la question et pistes de recherche, Bulletin de l'Association Pro Aventico 51, 7-57.
2. Krieg, M. (2009) Conservation-restauration de fragments de cadre d'un lit romain en bronze. Travail de semestre, filière Conservation-restauration, Haute Ecole Arc de Conservation-restauration, La Chaux-de-Fonds.
3. Krieg, M. (2012) Bis ans Ende der Patina. Vergleichende Untersuchungen von Grundmetall und Patina archäologischer Kupferlegierungs-Objekte aus Avenches (VD). Master thesis, unpublished. Hochschule der Künste Bern.
4. Krieg, M. (2015) Vergleichende Untersuchungen von Grundmetall und Patina archäologischer Objekte aus Kupferlegierung aus "Avenches" (Avenches). In: 18th International Congress on Ancient Bronzes, Deschler-Erb, E. and Della Casa, P. (eds), New Research on Ancient Bronzes, Zurich Studies in Archaeology, 10, 275-280.

Reference sample

5. Krieg, M. (2009) Conservation-restauration de fragments de cadre d'un lit romain en bronze. Travail de semestre, filière Conservation-restauration, Haute Ecole Arc Conservation-restauration, La Chaux-de-Fonds.

References on analytic methods and interpretation

6. Bouchard, M., Smith, D.C. (2003) Catalogue of 45 reference Raman spectra of minerals concerning research in art history or archaeology, especially on corroded metals and coloured glass. Spectrochimica Acta, Part A 59, 2247-2266.
7. Robbiola, L., Blengino, J-M., Fiaud, C. (1998) Morphology and mechanisms of formation of natural patinas on archaeological Cu-Sn alloys, Corrosion Science, 40, 12, 2083-2111.

This work is licensed under CC BY-NC-ND 4.0